Journal of Applied Research and Technology

www.jart.ccadet.unam.mx
Journal of Applied Research and Technology 16 (2018) 404-421

Original

# Application of natural minerals for *in-situ* catalytic pyrolysis of orange peel

Daniela Xulú Martínez-Vargas [a], Ladislao Sandoval-Rangel [a], Carolina Solís-Maldonado [b], Javier Rivera De La Rosa [c], Carlos J. Lucio-Ortiz [c], Gloria Dimas-Rivera [c], Norma A. Ramos-Delgado [d], Alberto Mendoza-Domínguez [a],*

[a] *Tecnológico de Monterrey, Escuela de Ingeniería y Ciencias, 64849*

[b] *Universidad Veracruzana, Facultad de Ciencias Químicas, 93390*

[c] *Universidad Autónoma de Nuevo León, Facultad de Ciencias Químicas, 64451*

[d] *Instituto Tecnológico de Nuevo León, Centro de Investigación e Innovación Tecnológica, 66629*

Received dd mm aaaa; accepted dd mm aaaa
Available online dd mm aaaa

**Abstract:** Natural mineral catalysts dolomite and clinoptilolite were evaluated in their calcined and non-calcined form for application in the catalytic *in-situ* pyrolysis of orange peel. Biomass pyrolysis improved when using calcined catalysts, with an increase in biogas yields (5.4 and 5.2% increase for dolomite and clinoptilolite, respectively), while non-calcined catalysts promoted higher condensate yields with an increment of 21.3 and 16.2% for dolomite and clinoptilolite compared with the calcined catalyst tests. Characterization of the condensate fraction with GC-MS showed formation of less oxygenated organic molecules in the pyrolysis tests, with an increase of 66% and 139% in the relative areas of organic compounds with an atomic content lower than 20%, when calcined dolomite and clinoptilolite were used, respectively, compared with the non-calcined catalysts. A prominent formation of Limonene was also observed. Syngas analysis with GC-TCD showed calcined clinoptilolite promoted higher hydrogen contents, while calcined dolomite showed increased CO and $CO_2$ production at the highest pyrolysis temperatures. The presence of catalyst almost always promoted higher primary gas generation when compared with the non-catalytic test. The kinetic study of the catalytic pyrolysis of orange peel showed calcination of the natural minerals promotes a decrease in the apparent activation energy and an increase in the kinetic constant of the process, which shows the promising application of natural minerals as catalysts for biomass pyrolysis applications.

*Keywords:* Pyrolysis, Catalysis, Natural Minerals, Biomass

## 1. INTRODUCTION

Because of exponential growing population, food demand is increasing, which in turn considerably increases agroindustrial wastes, becoming a relevant environmental problem. In addition to this, a greater coverage of services and products is also required, which leads to a search for alternatives and new sources of energy and raw materials.

Citrus fruit crops are the most abundant in the world (~120 million tons), where orange is the main product (Luengo, Álvarez, & Raso, 2013). Mexico is currently a leader in citrus production, being the fifth largest producer

* Corresponding author.
*E-mail address:* mendoza.alberto@itesm.mx (Alberto Mendoza-Domínguez).

Peer Review under the responsibility of Universidad Nacional Autónoma de México.

http://

worldwide (4.6% of the total). Citriculture is an important social and economic activity, which is carried out on 23 states, of which the most important are Veracruz, San Luis Potosí, Tamaulipas, Puebla and Nuevo León (Bridgwater, 2006; SAGARPA, Secretary of Agriculture, Livestock, Rural development, n.d.).

Peels are the major solid waste of orange processing and represent about half of the fruit weight (Kantar et al., 2018; Li, Smith, & Hossain, 2006; Lopez-Velazquez, Santes, Balmaseda, & Torres-Garcia, 2013a; Maran, Sivakumar, Thirugnanasambandham, & Sridhar, 2013). As a consequence, it is one of the main wastes of the juice industry. These residues, without a well-defined application, may result in environmental disasters due to improper disposal (Marshall & Farahbakhsh, 2013).

Biomass has been considered as a viable energy source and also as an alternative for the generation of raw materials produced from oil nowadays. Citrus agroindustrial residues are abundant and inexpensive material which can be used as biomass and therefore, as a sustainable alternative to solve an environmental and energy problem. Orange peels can be used as biomass for the production of high value-added products and fuels (Bridgwater & Peacocke, 2000; Ranzi et al., 2008). One of the most abundant agroindustrial wastes in Nuevo León state is sweet orange (*Citrus sinensis*) peel (Suárez-Jacobo et al., 2017).

Biomass conversion can be achieved by biological and thermochemical processes; the main difference between biological and thermal conversions is that biological conversion is a slow process with single or specific products such as ethanol or biogas, while thermal conversion takes place in short times and gives a variety of products (with potential to fuels or high-valued chemicals) and usually a catalyst is employed to upgrade the quality of the products (Bridgwater & Peacocke, 2000).

The main thermochemical processes used for biomass conversion are direct combustion, gasification and pyrolysis. Gasification and pyrolysis allow a greater valorization of the biomass and usually have high conversion efficiencies, potentially competitive costs, and considerable flexibility in scale of operation and range of products (Bridgwater & Peacocke, 2000). Furthermore, pyrolysis is the most versatile process due to the fact that solid (bio-char), liquid (bio-oil) and gaseous products are obtained and its application has the potential to diversify the energy-supply leading to a more secure and sustainable global energy-supply chain (Lopez-Velazquez et al., 2013a). The quality of pyrolysis bio-oil from lignocellulose material as orange peel is too poor for direct use as fuel or fuel precursor (Babich et al., 2011; Lazdovica, Liepina, & Kampars, 2015). This bio-oil is usually characterized by its high viscosity, acidity, instability and low energy density, generally due to the presence of highly oxygenated compounds (Aho et al., 2008; Babich et al., 2011; Kelkar et al., 2014; Lazdovica et al., 2015; D. Wang, Xiao, Zhang, & He, 2010). Consequently, an upgrading process is necessary for the bio-oil before being used as a regular fuel, mainly involving the removal of oxygen in the bio-oils in order to decrease its acidity, which leads to an energy density increase (Demiral & Sensöz, 2008; Lazdovica et al., 2015; Pütün, Uzun, & Pütün, 2006; Wang et al., 2010). Catalytic pyrolysis has been suggested as an alternative to the direct conversion of biomass into high quality liquid bio-fuels (Kim et al., 2017; Lazdovica et al., 2015; Lazdovica, Liepina, & Kampars, 2016).

One of the methods used for bio-oil upgrading (usually promoting deoxygenation) is catalytic cracking (with zeolites, aluminosilicates and molecular sieves) (Bridgwater, 1996; Vitolo, Seggiani, Frediani, Ambrosini, & Politi, 1999), with the economic advantage that $H_2$ is not required for hydrotreating (Huber & Corma, n.d.).The use of a suitable catalyst might change the reaction system during the pyrolysis process and result in an *in-situ* upgrading of the bio-oil. Heterogeneous catalysts are promising and adequate for use at pyrolysis conditions (450-550 °C) (Babich et al., 2011; Helwani, Othman, Aziz, Fernando, & Kim, 2009; Kelkar et al., 2014; Kersten, van Swaaij, Lefferts, & Seshan, 2007). The most studied catalysts in catalytic pyrolysis of biomass have been synthetic acid zeolites, mainly ZSM-5 (Aho et al., 2008; French & Czernik, 2010; Kelkar et al., 2014; Kim et al., 2017; Lazdovica et al., 2015, 2016; Li et al., 2014) and others such as MCM-41 (Adam et al., 2006; Antonakou, Lappas, Nilsen, Bouzga, & Stöcker, 2006; Iliopoulou, E.V. Antonakou, Karakoulia, Vasalos, Lappas, 2007), MFI (Kelkar et al., 2014), Beta (Aho et al., 2007, 2008), Y (Aho et al., 2008; Nguyen, Zabeti, Lefferts, Brem, & Seshan, 2013) and mordenite (Aho et al., 2008) resulting in selectivity improvement by decreasing the content of oxygenated compounds, which promoted a better performance in the production of aliphatic and aromatic hydrocarbons (Aho et al., 2007; Atutxa, Aguado, Gayubo, Olazar, & Bilbao, 2005; Horne & Williams, 1996; Kelkar

et al., 2014; Lappas, Samolada, Iatridis, Voutetakis, & Vasalos, 2002; Yaman, 2004) . Some authors (Kim et al., 2017; Zhang et al., 2014) have previously proposed modification of the neutral SBA-15 as an alternative to zeolite use for biomass pyrolysis applications due to its higher thermal and hydrothermal stability . Furthermore, the use of low-cost materials such as dolomite and limestone has been reported, upgrading the pyrolysis oils to obtain higher liquid yields (Nokkosmäki, Krause, Leppämäki, & Kuoppala, 1998). Babich *et al.* (Babich et al., 2011) reported that $Na_2CO_3$ catalyst increases the heating value while decreasing the acidity of the bio-oil. CaO and dolomite have also been employed as tar cracking catalysts in thermal decomposition (Conesa & Domene, 2015; Wang et al., 2010), Wang *et al.* (Wang et al., 2010) tested CaO in the pyrolysis of catalytic corncob, resulting in effective deacidification, which in turn enhanced hydrocarbons production.

In this research, *in-situ* catalytic pyrolysis was studied, employing cheap, local minerals such as dolomite and clipnoptilolite as catalysts, being an attractive alternative to synthetic catalysts. In order to address not only a global environmental problem but also a local one, sweet orange (*Citrus sinensis*) peel (just the peel and not pulp) was chosen as biomass, being one of the most abundant agroindustrial wastes in Nuevo León state. The catalysts were tested for *in-situ* catalytic pyrolysis in their calcined and non-calcined form. Catalysts and the generated syngas and bio-oils were characterized.

## 2. EXPERIMENTAL

### 2.1 BIOMASS

Sweet orange (*Citrus sinensis*) peels were obtained from a local market. The biomass was dried in an oven at 60 °C for 24 h, prior to any further study. The dried biomass was grinded and sieved to a particle size between 250 and 2000 μm.

### 2.2 CATALYSTS

Dolomite and clinoptilolite were provided by local businesses (Desarrollo Ambiental Máximo and Grupo Filtrantes). Quartz sand (Sigma-Aldrich) was used as non-catalytic material. The catalysts were all grinded and sieved to a particle size between 250 and 2000 μm, and stored at 60 °C before use. To study the effect of catalyst calcination, these minerals were calcined at 800 °C for 4 hours. The calcination procedure consisted in heating at 800 °C for 4 h, and was performed using a microwave muffle furnace (CEM Phoenix). At the end, both non-calcined and calcined catalysts were collected. Therefore, four catalysts were obtained: non-calcined dolomite (NC-Dolomite), calcined dolomite (C-Dolomite), non-calcined clinoptilolite (NC-Clinoptilolite) and calcined clinoptilolite (C-Clinoptilolite).

### 2.3 CHARACTERIZATION OF BIOMASS AND CATALYSTS

#### 2.3.1 Characterization of biomass and biomass-catalyst mixtures

To prepare the biomass-catalyst mixtures, catalysts were mecanically mixed with the dried biomasses and sieved to a particle size of $< 2$ mm. The thermochemical behavior of the mixtures of biomass with quartz sand (non-catalytic test) and the different catalysts was evaluated using thermogravimetric (TG) analysis coupled with differential scanning calorimetry (TGA-DSC, Linseis TGA-PT1000 model). In all cases, the ratio of biomass to catalyst used for the mixtures was 1:1. The conditions used for the thermogravimetric studies were heating from 25 to 750 °C (10°C/min ramp), with a nitrogen flow of 100 mL/min, 20 mg samples, with a particle size between 250 and 2000 μm.

#### 2.3.2 Characterization of catalysts

The nature of functional groups in the catalysts was analyzed with Fourier-transform infrared spectroscopy (FTIR), using a Perkin Elmer Frontier instrument. Samples were analyzed using an attenuated total reflectance (ATR) accessory. The software used for spectra management was Spectrum (Perkin Elmer), in transmittance mode. All spectra were acquired with 64 scans and using a resolution of 4 $cm^{-1}$. The wavenumber range of the tests was from 4000 to 350 $cm^{-1}$.

In order to evaluate the presence of crystalline phases, the calcined and non-calcined catalysts were characterized by X-ray diffraction (XRD) using a Siemens model D-5000 diffractometer. The measurements were performed using Cu Kα radiation in the 2θ range of 5-80°, with a 0.020° step every 4 seconds, at 25 °C. The pH of the catalysts was recorded according to the methodology described by Gurevich et al (Messina, Bonelli, & Cukierman, 2017),

with a pH-meter (Orion 3 Star). Scanning electron microscopy (SEM), Zeiss EVO MA25 microscope, coupled with a Bruker XFlash 6110 energy dispersive X-ray spectrometer (EDX) was used to elucidate the morphology and the composition of the different catalysts.

### 2.4 IN-SITU CATALYTIC PYROLYSIS TESTS

The reactor setup used for the *in-situ* catalytic pyrolysis experiments consisted in a bench-scale stainless-steel semi-continuous reactor, where a biomass-catalyst mixture sample was placed in the bottom and heated from room temperature to a maximum of 600 °C, at an approximate heating rate of 10 °C/min. The generated biogas flowed through the system on its own. At the immediate exit of the pyrolysis reactor, a heated stainless-steel tube was placed, which was maintained at 70 °C during the experiments, in order to avoid early condensation of the bio-oils. After the heated tube, a Büchner flask was present, which was cooled at a constant temperature of 3 °C with ice in order to properly condensate the generated bio-oil. The non-condensable compounds continued flowing, first through two glass tubes (impactors) which were also cooled at 3 °C and acted as a trap for organic products which could have exited the Büchner flask without condensing. After the impactors, the gas continued flowing through a sampling port and finally the vent. A total sample mass of 200 g (biomass:catalyst ratio of 1:1) was used in all tests. The condensed fractions were collected in the aforementioned Büchner vacuum flask, and then transferred to individual glass bottles and stored at 3 °C in absence of light for further analysis. Biogas was obtained from the sampling port and stored in Tedlar bags at three different temperature ranges: 200 – 290 °C (15 min, Temperature 1), 300 – 340 °C (5 min, Temperature 2), and 380 – 490 °C (15 min, Temperature 3), according to the data obtained by the TG tests.

### 2.5 CHARACTERIZATION OF THE PYROLYSIS PRODUCTS

Gas chromatography coupled to a thermal conductivity detector (GC-TCD) was used in order to evaluate the content of primary gases such as $H_2$, CO, $CO_2$ and $CH_4$ in the syngas. The instrument used was a Hewlett Packard 5890 Series II, which operated using a custom column with the characteristics: 15' 1/8" SS column, Carboxen 1000 resin, 60/80.

In order to separate the organic phase (bio-oil) from the condensate fraction, a liquid-liquid extraction was performed using dichloromethane (Tedia, HPLC grade) as solvent. The bio-oil:solvent ratio used was 1:2 (volume). The extracted organic phase was evaluated using gas chromatography coupled to mass spectrometry (GC-MS), with an Agilent 6890 series gas chromatograph, coupled to a MS 5973 Network mass selective detector. An HP5-MS (Agilent) column was used, and the $m/z$ range was 30-550. Helium (99.997%) was used as eluent gas for the GC-TCD and GC-MS tests.

## 3. RESULTS AND DISCUSSION

### 3.1 FTIR SPECTROSCOPY

Figure 1 shows the FT-IR spectra of the mineral catalysts before and after calcination. For NC-Dolomite and NC-Clinoptilolite, characteristic bands are observed for stretching vibrations in the range of 3000-3600 $cm^{-1}$ (Figure 1a,c) (Ji, Ge, Balsam, Damuth, & Chen, 2009; Korkuna et al., 2006; Lavat, Grasselli, & Lovecchio, 2015) and for bending vibrations at 1640 $cm^{-1}$ (Figure 1a) for NC-Dolomite and 1625 $cm^{-1}$ for NC-Clinoptilolite (Figure 1a) (Ji et al., 2009; Lavat et al., 2015); this due to adsorbed surface water, for both catalysts. As expected, after calcination, water is eliminated from the surface of the minerals; for C-Dolomite and C-Clinoptilolite the aforementioned signals disappear (Figure 1b, d).

In Figure 1a,b, the signals at 1423 and 1437 $cm^{-1}$ are associated with assymetric C-O vibrations from the carbonate group (Correia et al., 2015; Lavat et al., 2015; Sasaki, Yoshida, Ahmmad, Fukumoto, & Hirajima, 2013); in the same case, the bands at 879 and 875 $cm^{-1}$ are related to bending vibrations of the $CaCO_3$ groups in dolomite (Lavat et al., 2015). For NC-Dolomite (Figure 1a), a band is observed at 853 $cm^{-1}$, which is attributed to bending vibrations of both the $CO_3^{2-}$ group outside the plane (Correia et al., 2015) and the Mg-C bond (Jarrahian, Seiedi, Sheykhan, Sefti, & Ayatollahi, 2012; Sasaki et al., 2013) present in dolomite. On the other hand, the signal at 728 $cm^{-1}$ is related to bending vibrations from the $CO_3^{2-}$ functional group inside the plane (Correia et al., 2015; Ji et al., 2009) and the Ca-C bond (Jarrahian et al., 2012; Sasaki et al., 2013). These signals are absent in the C-Dolomite spectrum, or they may be present with a significantly decreased intensity, since after calcination at 800 °C, the carbonate groups in dolomite ($CaMg(CO_3)_2$)

are eliminated, leading to formation of the CaO and MgO oxides (Sasaki et al., 2013).

The bands in the range of 1400-1500 $cm^{-1}$ are attributed to stretching vibrations of the C-O bond in the $CO_3^{2-}$ group for NC-Dolomite; when dolomite is heated above 700 °C, these signals are associated with $CaCO_3$ and the $CO_2$ formed by dolomite decomposition (Ji et al., 2009; Sasaki et al., 2013). The produced $CO_2$ is initially adsorbed in the CaO and/or MgO structures. However, above 800 °C, complete carbonate decomposition has been reported, and $CO_2$ is no longer adsorbed in the calcium and magnesium oxides (Sasaki et al., 2013). The bands at 1444 and 1145 $cm^{-1}$ are attributed to the $SiO_4$ present (Lavat et al., 2015). A significant decrease in signal intensity is clearly observed for C-Dolomite, while other bands completely disappear in comparison with NC-Dolomite; this is a consequence of structural transformations and decarbonation.

Since clinoptilolite is mainly composed by $SiO_2$ and $Al_2O_3$, the bands presented in this catalyst (before and after calcination) are related mainly to vibrations of the Si-O and Al-O bonds. The signals at 1000 cm-1 are associated to these event, and its position is related with the Si/Al ratio (Favvas et al., 2016). In the clinoptilolite spectra (Figure 1c,d) no significant change was observed related to a change in the band position for NC-Clinoptilolite and C-Clinoptilolite, therefore, no evidence is present of a change in the Si/Al ratio, which was later confirmed in the EDX results.

In Figure 1c,d, bands present in the 1200-400 $cm^{-1}$ range are associated with Si-O(Si) and Si-O(Al) bonds vibrations (Korkuna et al., 2006), while the signals in the range of 500-700 $cm^{-1}$ are attributed to pseudo-lattice vibrations. Bands below the 400 $cm^{-1}$ line are related with lattice vibrations [43]. Finally, the signals at 420-500 $cm^{-1}$ represent bending vibrations from the Si-O and Al-O bonds (Perraki & Orfanoudaki, 2004).

### 3.1 XRD

Crystalline phases present in calcined and non-calcined natural mineral catalysts were detected by XRD. Figure 2a shows the diffraction pattern for NC-Dolomite, where the main dolomite $MgCa(CO_3)_2$ phase is observed (Charusiri & Vitidsant, 2017; Elbaba & Williams, 2013; Paulo & Dittrich, 2013; Xie et al., 2016). The presence of other phases such as aragonite and calcite ($CaCO_3$ phases), $MgCO_3$, CaO, halite (NaCl) and quartz were also observed (Paulo & Dittrich, 2013). For C-Dolomite, disappearance of the carbonate phases is observed (except calcite, the most stable phase), with the appearance of high-magnesium calcite, CaO and MgO phases (Charusiri & Vitidsant, 2017; Elbaba & Williams, 2013); quartz signals remain present after calcination. The observed phase changes occur due to transformation of dolomite to Ca and Mg oxides, promoted by the calcination treatment.

Clinoptilolite is mainly formed by aluminosilicates, where the microstructure comprehends a tetrahedron tridimensional lattice formed by $SiO_4$ and $AlO_4$, with silicon and aluminum atoms at the center and oxygen atoms at the corners (Faghihian, Talebi, & Pirouzi, 2008); other elements may be present, since $AlO_4$ excess promotes local negative charges which are neutralized with cations such as $Na^+$, $K^+$, $Ca^{2+}$, $Sr^{2+}$, $Mg^{2+}$, etc., via electrostatic forces (De J. Montes Luna et al., 2018; Olguín Gutiérrez, 2007). The obtained diffraction pattern for NC-Clinoptilolite is in agreement with previous reports by other authors for natural zeolites of the clinoptilolite type (Adriano Macas, 2012; Favvas et al., 2016; Korkuna et al., 2006; Rodríguez-Méndez et al., 2014); it also presents quartz as impurity (common in natural minerals), which remains in the diffraction pattern after calcination. However, characteristic natural zeolite diffraction peaks mostly disappear after the thermal treatment, this may be due to the collapse of the zeolite structure, loss of crystallinity and formation of amorphous phases (J.-C. Kim et al., 2014). Quartz may form as product of temperature increase; the complete zeolite structure decomposition temperature is 900 °C, which is the reason why some clinoptilolite phase peaks are still present in the diffraction pattern of C-Clinoptilolite (Guvenir, 2005).

### 3.2 SEM

The morphology of the mineral natural catalysts, both in their calcined and non-calcined form, was evaluated. Figure 3 shows the SEM micrographs, where dolomite shows rounded particles and a heterogeneous particle size distribution (Correia et al., 2015; Sasaki et al., 2013); small aggregates are observed over the bigger-size particles. In the C-Dolomite micrograph (Figure 3b), a higher amount of aggregates and smaller particles are observed, in comparison with the image for NC-Dolomite (Figure 3a), which is in agreement with previous works, which report a decrease in particle size when dolomite is calcined above 600 °C (Sasaki et al., 2013). For NC-Dolomite, smooth

particles are observed, while after calcination roughness increases, along with the pores and smaller aggregates amount (over the bigger particles), which again agrees with previous reports (Correia et al., 2015; Lavat et al., 2015; Sasaki et al., 2013). This may be observed due to an increase in surface area and porosity after calcination due to decomposition of Ca and Mg carbonates, which promote pore forming after $CO_2$ desorption from CaO and MgO sites. Therefore, calcination enhances the structural properties of dolomite, which may increase the catalytic properties of this material.

Non-calcined clinoptilolite (Figure 3c) presented a morphology which consisted in plates and ribbons, as reported for natural clinoptilolite present in sedimentary rocks. Rounded particles are also observed, and the particle size distribution appears to be similar to that of dolomite (Guvenir, 2005). C-Clinoptilolite presents a morphology similar to that of NC-Clinoptilolite, with a clear decrease in the presence of ribbon-shaped particles over bigger particles, which in turn show a smoother surface. These may be related to thermal decomposition, where the zeolitic structure partially collapses, since the temperature at which the structure is completely destroyed is 900 °C (Guvenir, 2005; Sasaki et al., 2013). This was confirmed in the diffraction patterns previously discussed in Section 3.2.

### 3.3 EDX

Figure 4 shows the energy dispersive X-ray spectra for the calcined (Figure 4b,d) and non-calcined (Figure 4a,c) catalysts, along with the elemental surface compositions. The chemical composition of dolomite is $CaMg(CO_3)_2$; however, other elements are present as impurities due to the natural origin of the mineral. The EDX analysis showed that for C-Dolomite, oxygen content decreases, while Mg and Ca distributions increase. This is directly related with the decarbonation process, where $CO_2$ is released by thermal decomposition of the Mg and Ca carbonates (Algoufi, Kabir, & Hameed, 2017). This confirms the previous evidence found in the previously discussed results of FTIR and XRD.

Clinoptilolite is mainly composed by aluminosilicates; however, some cations such as $Na^+$, $K^+$, $Ca^{2+}$, $Sr^{2+}$ and $Mg^{2+}$ may also be present (De J. Montes Luna et al., 2018). The EDX analysis shows a higher Ca content for NC-Clinoptilolite compared with previous reports (Favvas et al., 2016; Messina et al., 2017); this causes a reduction in the Si and Al contents, probably due to the presence of $CaCO_3$ and CaO. In the case of C-Clinoptilolite, an increase in Ca content is observed, with a decrease in the content of Si, Al and O, probably due to desilication and/or dealumination processes. This events may be the results of calcination and partial destruction of the crystalline zeolitic structure (Wang, Yokoi, Namba, & Tatsumi, 2016).

### 3.4 THERMOGRAVIMETRIC ANALYSIS

#### 3.4.1 Thermal behavior

Figure 5 shows the thermogravimetric analysis for the non-catalytic and catalytic biomass mixtures. The dTG curves (Figure 5b) clearly show the presence of three main decomposition events, their temperature ranges were identified as: 200-290 °C, 300-340 °C and 380-490 °C. According to these results, the same temperature sampling ranges were used in the catalytic *in-situ* pyrolysis tests performed in the semi-continuous reactor.

Figure 5a shows the TG curves, where the mass decrease below 120 °C is associated with physisorbed water desorption, and possibly water-soluble species that volatilize at low temperatures (Lopez-Velazquez et al., 2013a; Miranda, Bustos-Martinez, Blanco, Villarreal, & Cantú, 2009a; Santos, Dweck, Viotto, Rosa, & de Morais, 2015). Two overlapping steps (corresponding to a mass loss of approximately 20%) are observed in the range of 160-300 °C, which may be attributed to initial hemicellulose and partial cellulose decomposition (Lopez-Velazquez et al., 2013a; Miranda et al., 2009a). At the temperature range of 300-600 °C, at least two slope changes are observed, which correspond to overlapping mass-loss stages associated with completion of hemicellulose decomposition, ongoing cellulose decomposition and lignin degradation (Lopez-Velazquez et al., 2013a; Santos et al., 2015); this stage shows a mass loss between 25-30%. After 600 °C, complete degradation of the orange peels is expected, according to previous reports (Aguiar, Márquez-Montesinos, Gonzalo, Sánchez, & Arauzo, 2008; Kim et al., 2017).

According to literature, dolomite may show mass losses in the 600-850 °C range, due to the decarbonation process (Djayaprabha, Chang, Shih, & Chen, 2017), which is the process attributed to the additional mass loss event at the end of the TG curve for NC-Dolomite. For clinoptilolite, physisorbed water loss is observed until 200

°C, with continuous reticular water loss in the 200-700 °C range, which is characteristic of this type of natural zeolite in comparison with other more stable zeolites such as mordenite. This events may add to the mass loss of the biomass-catalyst mixtures (Ates & Hardacre, 2012).

### 3.4.2 Kinetic analysis

Model-free isoconversional methods have been reported in literature as useful for activation energy ($E_a$) calculations in thermally activated reactions (Starink, 2003). Therefore, two of these methods were used in this work, namely the Flynn-Wall-Ozawa (FWO) (Jain, Mehra, & Ranade, 2016; Venkatesh, Ravi, & Tewari, 2013) and Kissinger-Akahira-Sunose (KAS) (Jain et al., 2016; Lopez-Velazquez, Santes, Balmaseda, & Torres-Garcia, 2013b) methods. The Kissinger equation was also used to calculate the pre-exponential (A) factor, and the kinetic constant (k) was also obtained with the expression for Arrhenius Law (Jain et al., 2016; Urych, 2014). The final equations for the methods are resumed in Table 1, where β represents the heating rate in °C/min, α represents the conversion degree, T is the temperature in K and $T_{max}$ is the temperature associated with the maximum intensity of the events (peaks) observed in the DTG curves.

For the calculation of activation energies, TGA tests were performed at different heating rates (β): 5, 10 and 15 °C/min. In order to clearly evaluate the effect of the heating rate in the thermal events of orange peel pyrolysis, Figure 6 shows the DTG curves obtained for all three β values used. At least four important observations can be made from this plot: first, all DTG curves showed the same main behavior, with three main events clearly present in all cases, which may suggest the thermal behavior is independent of the heating rates. However, the intensity of the DTG peaks shows an inverse relation compared to the heating rate, with the maximum mg/K value decreasing with increasing β, which means the slope associated with mass loss becomes less pronounced. The sensibility of the DTG analysis also decreases with increasing heating rates, with small peaks overlapping with the main DTG events when β = 5 °C/min; however, at 10 °C/min, only the main peaks can be observed. At the final heating rate, even the two main events are overlapped with themselves. Finally, the logical shifting of the DTG peaks to higher temperatures with increasing β is also observed.

Figure 7 shows the results of the apparent activation energy calculations using the FWO and KAS methods previously described, for conversion degrees between 0.1 and 0.9. Almost identical results were obtained with the FWO and KAS equations, showing these two isoconversional methods closely describe the pyrolysis reactions performed in this work. Three maximum $E_a$ peaks were observed at 0.3, 0.6 and 0.8 conversion values, which are associated with the three main decomposition events previously identified in the DTG curves. It is very evident from these results that the non-catalytic test showed the highest $E_a$ values of all the mixtures. López-Velazquez *et al.* (Lopez-Velazquez et al., 2013b) reported apparent activation energies between 200 and 250 kJ/mol for pure orange peel samples, at similar α values. Since the Ea calculated for the non-catalytic test in this work varies between 600 and 1900 kJ/mol, this suggests the inert material in the mixtures negatively affect the pyrolysis process, blocking the biomass decomposition with quartz sand absorbing most of the termal energy to increase its temperature, therefore requiring higher energies for the orange peel to decompose. On the other hand, the catalytic mixtures showed a drastic decrease in the $E_a$ values, with maximums of 320 and 300 kJ/mol for conversion degrees of 0.6 and 0.8, respectively, observed in the mixture with NC-Zeolite. However, catalyst calcination promoted an even more marked apparent activation energy decrease, with values in the range of 130 and 145 kJ/mol for α = 0.6, and between 85 and 95 kJ/mol for α = 0.8, when C-Dolomite and C-Zeolite were present in the mixtures. These values are even lower than those reported by López-Velázquez *et al.*, which shows the calcinated catalysts have a positive effect on the $E_a$, which makes it more attractive to use them in mixtures with orange peels for pyrolysis applications than using the pure biomass.

The pre-exponential factor (A) was evaluated with the intersection value obtained from the regression equation calculated when plotting $\ln\left(\frac{\beta}{T_{max}}\right)$ versus $\frac{1}{T_{max}}$. Then the Arrhenius law was used to determine the kinetic constants.

Table 2 shows the kinetic parameters obtained, where peaks 1, 2 and 3 correspond to the main mass loss events observed previously in the DTG curves.

The kinetic constants suggest a modest effect of the catalysts on the reaction rate of orange peel pyrolysis.

However, a consistent behavior is also observed, with $k$ values increasing with calcination of the catalysts (except for Clinoptilolite in peak 2). C-Dolomite showed the highest $k$ values of all mixtures for the first two mass loss events.

To the best of our knowledge, this is the first time apparent activation energies are reported for catalytic pyrolysis tests, since most of the previous works have only worked with pure biomass samples or simple carbohydrates.

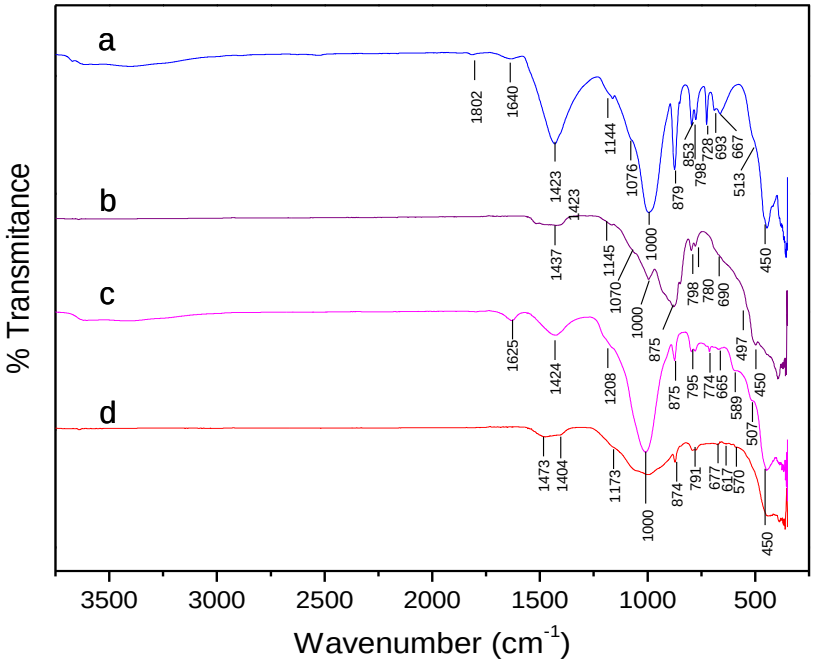


Fig. 1. FTIR spectra of pure mineral catalysts a. NC-Dolomite, b. C-Dolomite, c. NC-Clinoptilolite and d. C-Clinoptilolite.

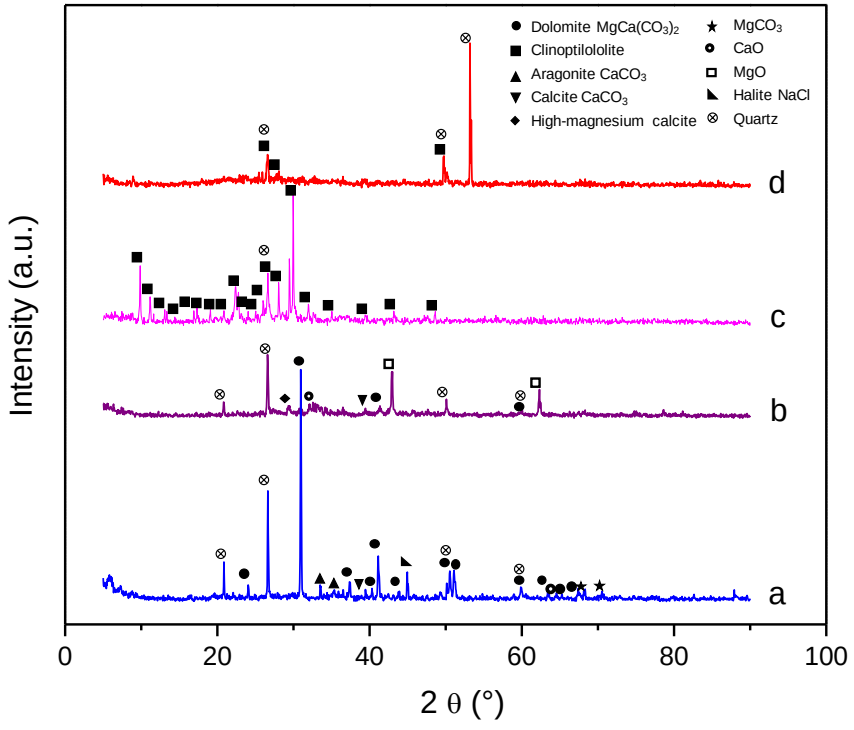


Fig. 2. XRD patterns of mineral catalysts a. NC-Dolomite, b. C-Dolomite, c. NC-Clinoptilolite and d. C-Clinoptilolite.

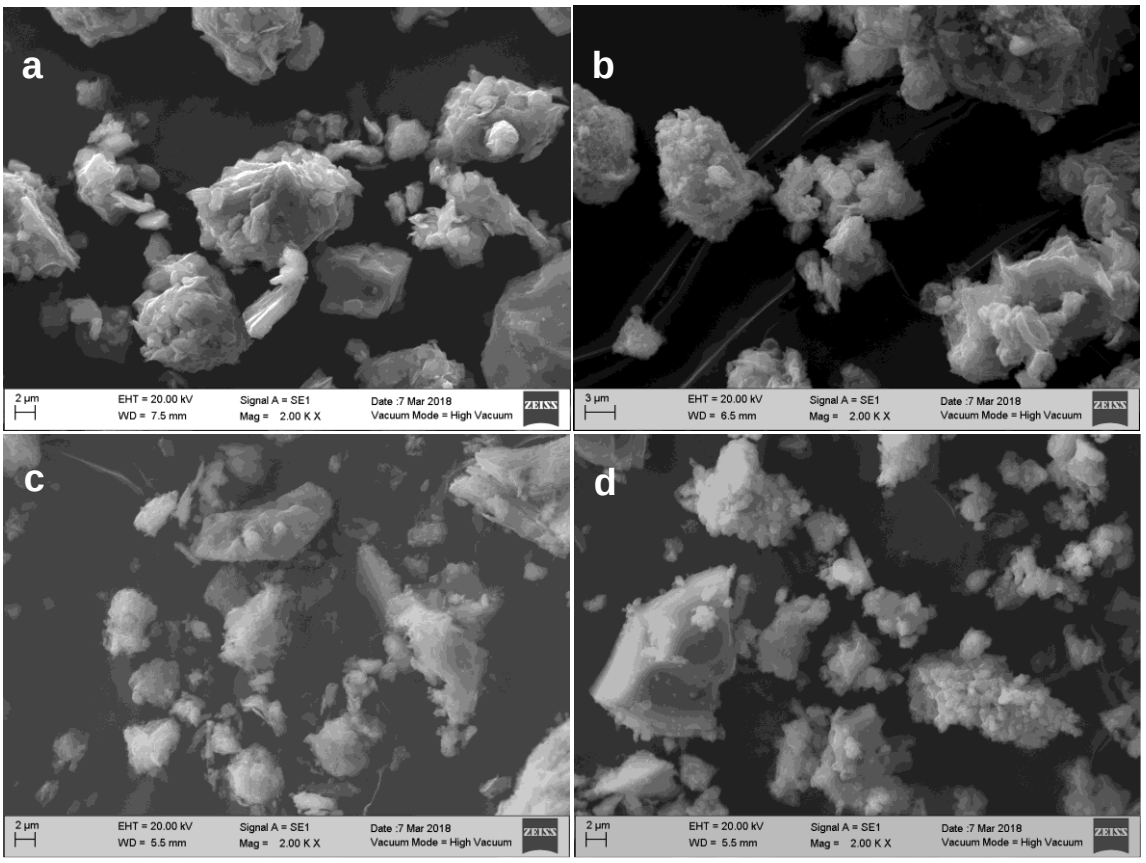


Fig. 3. SEM micrographs of natural minerals catalysts a. NC-Dolomite, b. C-Dolomite, c. NC-Clinoptilolite and d. C-Clinoptilolite. EHT: 20kV, Mag: 2.00k.

Table 1. Equations of isoconvertional methods used in this work.

| Method | Equation |
|---|---|
| FWO | $\ln\beta = ln\left(\frac{0.0048AE_a}{RG(\alpha)}\right) - 1.0516\frac{E_a}{RT}$ |
| KAS | $ln\left(\frac{\beta}{T^2}\right) = ln\left(\frac{AR}{E_a\,G(\alpha)}\right) - \frac{E_a}{RT}$ |
| Kissinger | $ln\left(\frac{\beta}{{T_{max}}^2}\right) = -\frac{E_a}{RT_{max}} + ln\left(\frac{AR}{E_a}\right)$ |

Table 2. Pre-exponential factors and kinetic constants values calculated with the method of Kissinger.

| | Peak 1 | | | Peak 2 | | | Peak 3 | | |
|---|---|---|---|---|---|---|---|---|---|
| **Sample** | **$A_1$ ($min^{-1}$)** | **$k_1$ ($min^{-1}$)** | **$R^2$** | **$A_2$ ($min^{-1}$)** | **$k_2$ ($min^{-1}$)** | **$R^2$** | **$A_3$ ($min^{-1}$)** | **$k_3$ ($min^{-1}$)** | **$R^2$** |
| Sand | 3.09E+04 | 0.2192 | 0.9899 | 6.89E+21 | 0.7818 | 0.8576 | 9.33E+13 | 0.4214 | 0.8122 |
| NC-Dolomite | 2.99E+04 | 0.2167 | 0.9900 | 6.89E+21 | 0.7818 | 0.8576 | 4.17E+03 | 0.1319 | 0.8833 |
| C-Dolomite | 5.79E+04 | 0.2296 | 0.9903 | 2.99E+38 | 1.3629 | 0.9906 | 6.10E+13 | 0.4128 | 0.9951 |
| NC-Clinoptilolite | 1.05E+04 | 0.2000 | 0.9949 | 1.55E+27 | 0.9721 | 0.9777 | 6.14E+04 | 0.1628 | 0.8391 |
| C-Clinoptilolite | 1.38E+04 | 0.2045 | 0.9894 | 1.55E+27 | 0.9721 | 0.9777 | 7.66E+08 | 0.2779 | 0.9090 |

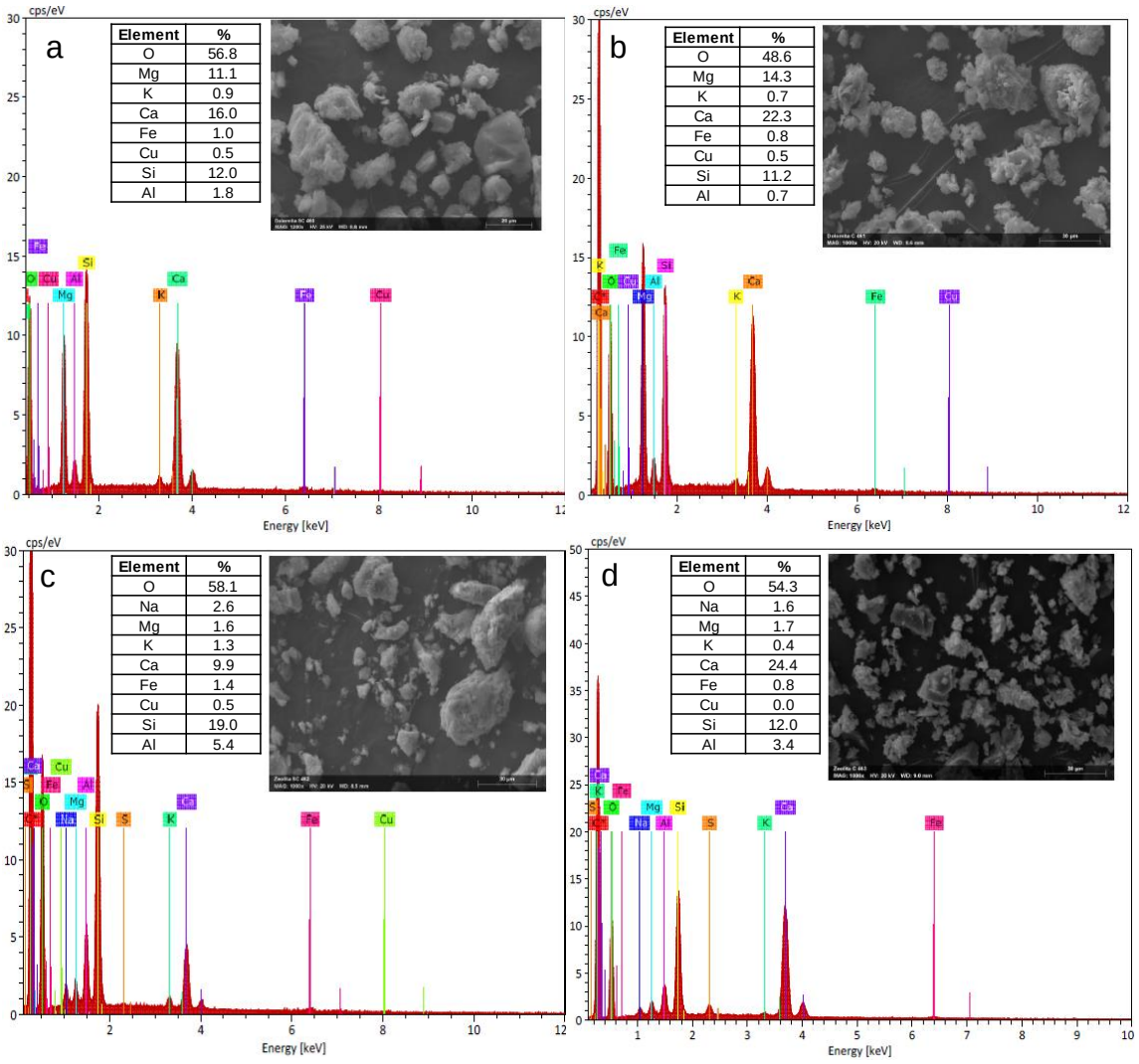


Fig. 4. EDX analysis of natural mineral catalysts a. NC-Dolomite, b. C-Dolomite, c. NC-Clinoptilolite and d. C-Clinoptilolite.

### 3.5 YIELDS OF IN-SITU CATALYTIC PYROLYSIS

Figure 8 shows product yields for the *in-situ* catalytic pyrolysis of orange peels, where the performance of different catalysts is compared with the non-catalytic test (quartz sand), where the values were calculated by mass balance. It is observed that calcination of the catalysts promotes an increase in syngas yield (5.4 and 5.2% increase for dolomite and clinoptilolite, respectively), likely due to bio-oil cracking deoxygenation (Bridgwater, 1996; Corma, Huber, Sauvanaud, & O'Connor, 2007; Vitolo et al., 1999). On the other hand, non-calcined catalysts showed selectivity for higher bio-oil production, with yields 21.3 and 16.2% higher for dolomite and clinoptilolite, when compared with the calcined materials. An increase in char yield is observed for the calcined catalysts; this was also observed in the TG results, and may occur due to $CO_2$ adsorption over the surface of CaO and MgO species formed after calcination (Sasaki et al., 2013). Therefore, higher selectivity for gases different tan $CO_2$ in the syngas may be expected. Though the yield increments may appear low, the main effect of the presence of catalysts in the mixtures was the product selectivity, which will be discussed in the next sections of this work.

Table 3 shows all organic compounds identified by GC-MS analysis of the bio-oils obtained from *in-situ* catalytic pyrolysis of orange peels, which are similar to results reported in previous works (Miranda, Bustos-Martinez, Blanco, Villarreal, & Cantú, 2009b). It was observed that for all cases, valuable chemical compounds

(building blocks) were generated. Cyclotene (compound widely used in fragrance and cosmetics industry, with world consumption calculated at 0.1-1 ton/year (Scognamiglio, Jones, Letizia, & Api, 2012) and guaiacol (model bio-oil molecule), used for biofuel synthesis (Pereira et al., 2018; Zhao, Li, Bui, & Oyama, 2011)) were found to be the main organic compounds found in the bio-oils generated from the non-catalytic and the catalytic tests where non-calcined materials were used. In the case of the calcined catalysts, the main product was D-Limonene, which is also widely used in the food, fragrancy, cosmetics and cleaning products industries, and has had a recent interest in the pharmaceutics area (Vieira, Beserra, Souza, Totti, & Rozza, 2018).

The non-catalytic test along with the pyrolysis tests performed with non-calcined catalysts showed a very prominent formation of highly oxygenated organic compounds (calculated by the mass percentage of oxygen in the molecule, and represented as %O in Table 2), with NC-Clinoptilolite having more than 39% of the relative area corresponding to organic compounds with more than 20% oxygen content, while NC-Dolomite and the non-catalytic test showed values of 53 and 58% for the same parameter, respectively. On the other hand, the percentage of relative area attributed to compounds with oxygen contents higher than 20% was only 18 and 25% for C-Dolomite and C-Clinoptilolite, respectively.

Therefore, calcination of the catalysts is observed to clearly promote formation of less-oxygenated compounds, which increased the quality of the generated bio-oils.

Loss of oxygen in the bio-oil is also associated with reduced acidity; Table 4 shows the pKa of most of the identified products. In general, formation of less acidic compounds was favored by the calcined catalysts. Figure 9 shows the results obtained by GC-TCD for the primary gases distribution ($H_2$, CO, $CH_4$, $CO_2$) in the obtained syngas for the previously described tests. A significant difference in hydrogen production (Figure 9a) was observed, where C-Clinoptilolite showed the highest values for all temperatures. In this case, the non-catalytic test showed hydrogen content results similar to that of the rest of the catalysts (except C-Clinoptilolite), while NC-Dolomite showed the lowest $H_2$ content in the syngas sampled at the highest pyrolysis temperature. A higher hydrogen production may be related with a higher calcium content present in C-Clinoptilolite, which was previously confirmed by EDX; previous works have reported pure CaO acts as pyrolysis catalyst, favoring water-gas shift reaction and methane reforming, with the consequent decrease in CO content in the syngas (Veses et al., 2014; Widyawati, Church, Florin, & Harris, 2011). A different behavior is therefore observed for CO content (Figure 7b), where while C-Dolomite shows the highest carbon monoxide values for the first two sampling temperatures, at the highest temperature CO production decreases, according to the previous discussion. Figure 9d shows all curves follow a similar trend, with $CH_4$ content increasing with higher temperatures. In this case, NC-Clinoptilolite showed the highest methane content at the highest sampling temperatures.

Table 3. Organic compounds distribution in the bio-oils, obtained with GC-MS.

| % O | Compound | % Relative area | | | | |
|---|---|---|---|---|---|---|
| | | Sand | NC Dolomite | C-Dolomite | NC-Clinoptilolite | C-Clinoptilolite |
| 38.1 | 2-Hydroxy-3-methylpyran-4-one | --- | 7.1 | --- | --- | --- |
| 38.1 | 5-Hydroxymethylfurfural | 4.9 | 6.3 | --- | --- | --- |
| 31.5 | 2,4-Dihydroxyacetophenone | --- | --- | --- | 4.0 | --- |
| 29.1 | Catechol | 8.0 | 5.9 | --- | 5.9 | 3.4 |
| 28.5 | Cyclotene | 17.4 | 12.3 | --- | 15.3 | 8.1 |
| 25.8 | Guaiacol | 12.6 | 13.8 | 10.1 | 12.3 | 5.7 |
| 25.8 | 3-Methyl catechol | 2.6 | --- | --- | --- | --- |
| 25.4 | Ethylcyclopentenolone | 7.1 | --- | 2.2 | --- | 2.3 |
| 23.5 | Methyl benzoate | --- | --- | --- | --- | 4.1 |
| 21.3 | 2-Metoxi-4-vinilphenol | 2.1 | 3.9 | 3.0 | 1.7 | 2.0 |
| 21.0 | 4-Ethylguaiacol | 3.3 | 3.6 | 2.8 | --- | --- |
| 14.8 | *o*-Cresol | 5.3 | 5.0 | --- | 8.3 | 2.1 |
| 14.8 | *m*-Cresol / *p*-Cresol | 6.9 | 7.0 | 7.3 | 8.5 | 3.4 |
| 14.7 | 3-Methoxypyridine | 5.5 | --- | --- | --- | 4.9 |
| 14.5 | 2,3-Dimethyl-2-cyclopenten-1-one | --- | 4.9 | 5.1 | 5.6 | 2.4 |
| 13.1 | 2,4-Dimethylphenol (*m*-Xylenol) | 5.3 | 6.7 | 7.0 | 5.4 | --- |
| 13.1 | 3,4-Dimethylphenol (*o*-Xylenol) | --- | 5.3 | --- | --- | --- |
| 13.1 | 4-Ethylphenol / 3-Ethylphenol | 3.7 | --- | 3.2 | --- | --- |
| 0.0 | Limonene | --- | --- | 25.4 | --- | 53.9 |
| | Not identified | 15.3 | 18.2 | 33.9 | 32.9 | 7.7 |

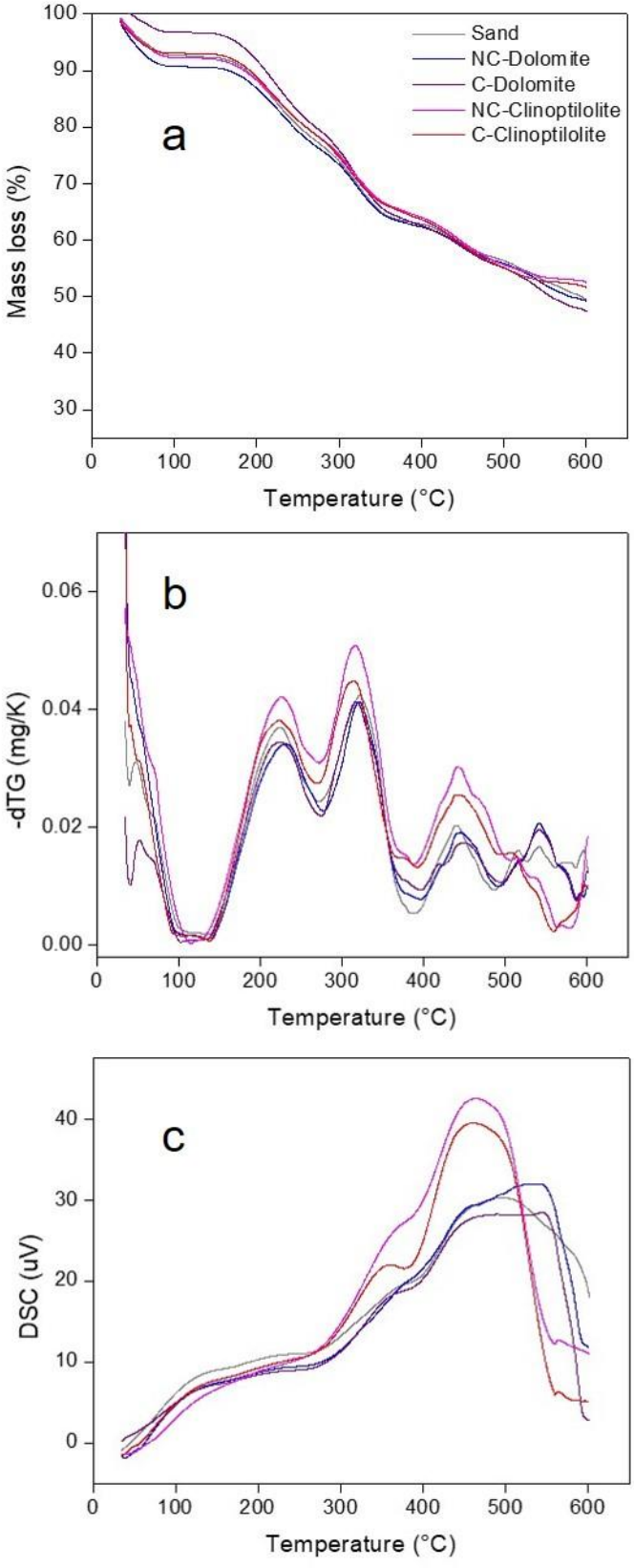


Fig. 5. Thermogravimetric analysis of orange peel mixtures with catalysts: a. TG, b. dTG and c. DSC. (Condi-tions: 20mg of sample; ramp: 10°C/min; flow rate: 100 mL $N_2$/min).

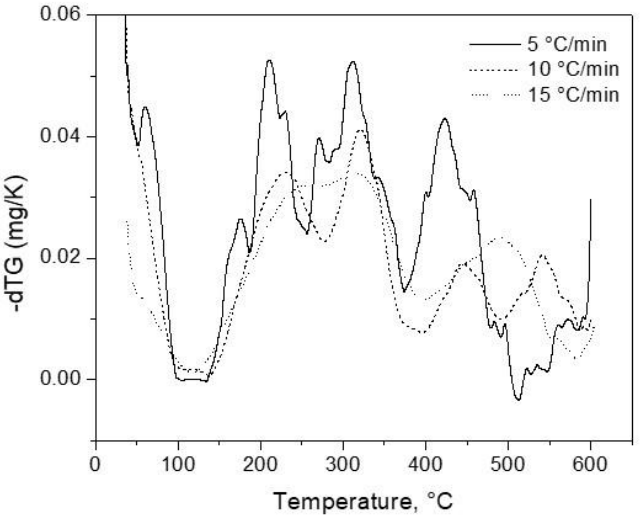


Fig. 6. DTG curves for the catalytic mixture of orange peel with NC-Dolomite at different heating rates.

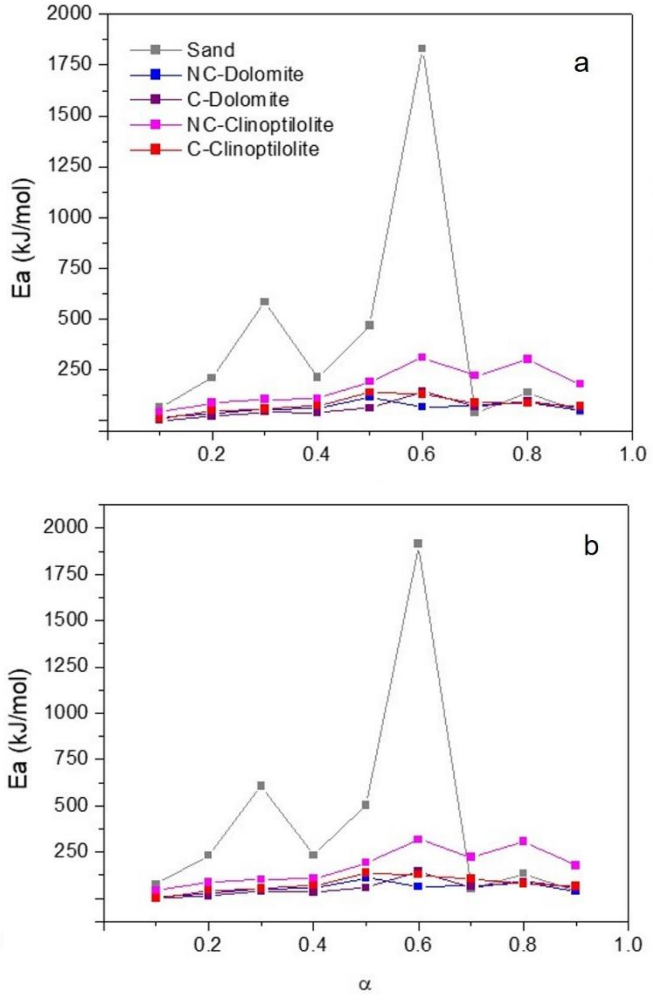


Fig. 7. Variation of the apparent activation energy Ea with the conversion degree, for different non-catalytic and catalytic mixtures of natural minerals with orange peels. Calculation performed by using: a. the FWO method, b. the KAS method.

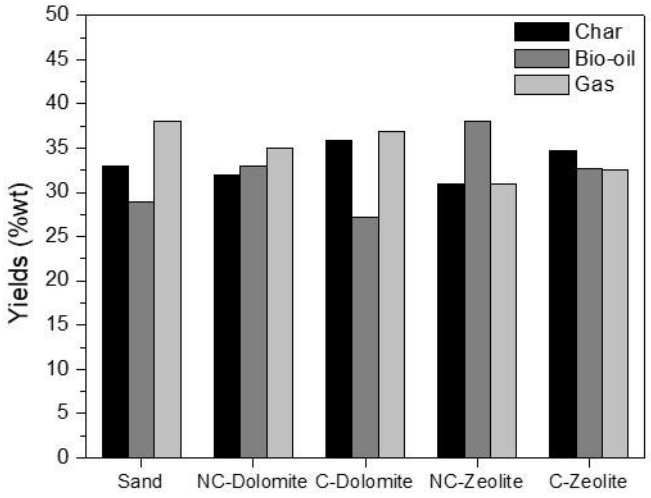


Fig. 8. Yields of the pirolitic products for non-catalytic pyrolisis and in-situ catalytic pyrolisis.

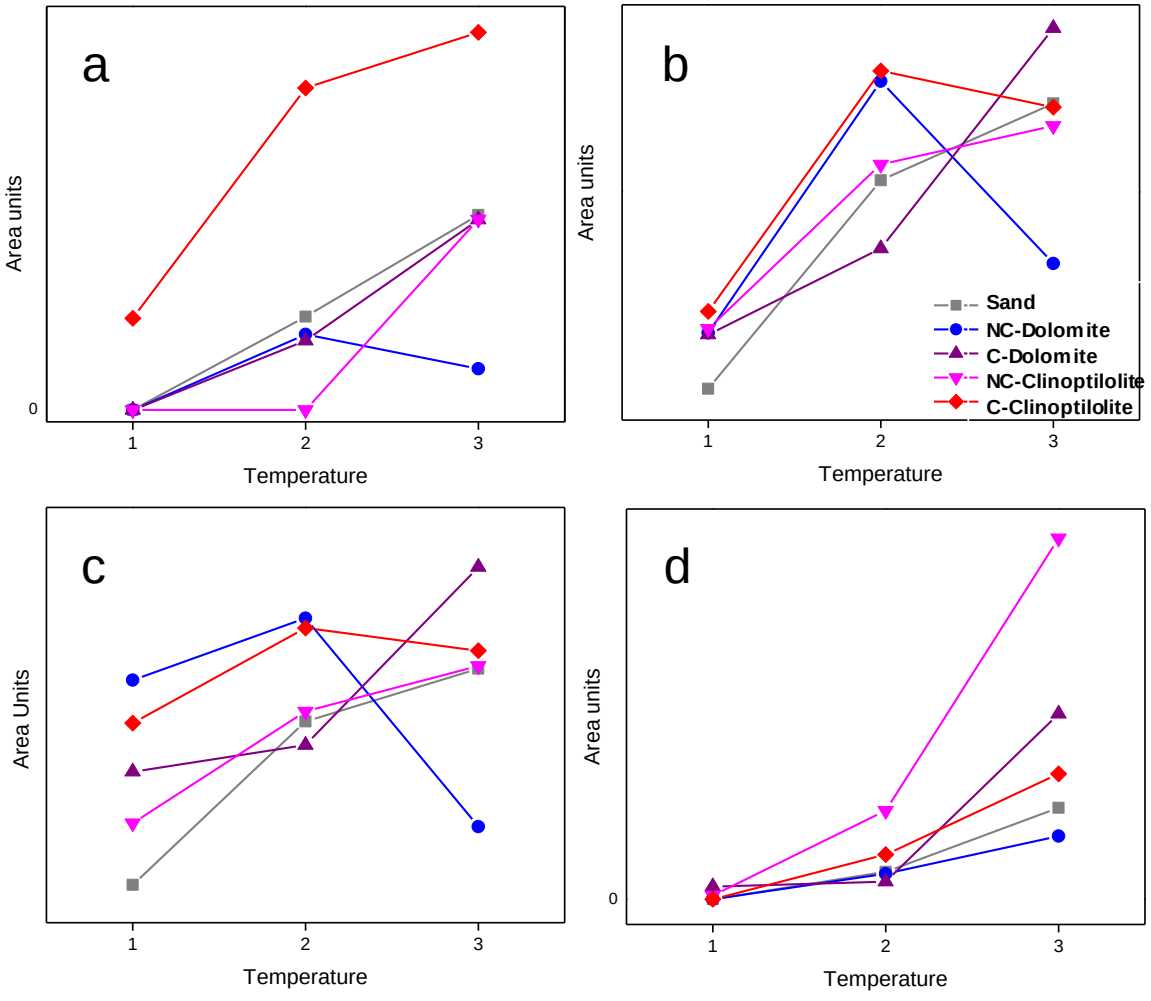


Fig. 9. Syngas components of *in-situ* orange peel catalytic pyrolisis at three different temperature ranges: a. $H_2$, b. CO, c. $CO_2$ and d. $CH_4$.

Table 4. Acidity values (represented by pKa) of the organic compounds identified by GC-MS.

| Compound | pKa | Ref. |
|---|---|---|
| **3-Methoxypyridine** | 4.8 | (Guillory, 2010) |
| **2,4-Dihydroxyacetophenone** | 7.9 | (Listing Compounds, n.d.) |
| **2-Hydroxy-3-methyl-2-cyclopenten-1-one (Cyclotene)** | 9.3 | (Yeast Metabolome Database,n.d.) |
| **3-Ethyl-2-hydroxy-2-cyclopenten-1-one (Ethylcyclopentenolone)** | 9.4 | (Listing Compounds, n.d.) |
| **2-Hydroxy-3-methylpyran-4-one** | 9.5 | (Listing Compounds, n.d.) |
| **Catechol** | 9.5 | (Serjeant & Dempsey, 1979) |
| **3-Methyl catechol** | 9.6 | (Listing Compounds, n.d.) |
| **4-Ethylphenol / 3-Ethylphenol** | 9.9 | (Pearce & Simkins, 1968) |
| **2-Metoxi-4-vinilphenol** | 10.0 | (Listing Compounds, n.d.) |
| **Guaiacol** | 10.0 | (Pearce & Simkins, 1968) |
| **4-Ethylguaiacol** | 10.3 | (Listing Compounds, n.d.) |
| **o-Cresol** | 10.3 | (Shiu, Ma, Varhaníčková, & Mackay, 1994) |
| **m-Cresol / p-Cresol** | 10.3 | (Pearce & Simkins, 1968) |
| **3,4-Dimethylphenol (*o*-Xylenol)** | 10.5 | (Listing Compounds, n.d.) |
| **2,4-Dimethylphenol (*m*-Xylenol)** | 10.6 | (Serjeant & Dempsey, 1979) |
| **5-Hydroxymethylfurfural** | 13.7 | (Listing Compounds, n.d.) |
| **2,3-Dimethyl-2-cyclopenten-1-one** | --- | --- |
| **Limonene** | --- | --- |
| **Methyl benzoate** | --- | --- |

## 4. CONCLUSIONS

In this work, the effect of the use of natural minerals and the impact of calcination treatment on these catalysts was studied. Impurities were found by XRD and EDX, while typical dolomite and clinoptilolite functional groups were identified by FTIR. SEM micrographs showed changes in particle size and morphology of the catalysts after calcination, while EDX confirmed the Si/Al remained intact after thermal treatment of the natural minerals, although some degree of desilication and dealumination was observed, especially in the case of clinoptilolite.

The presence of minerals slightly altered the mass-loss behavior, as observed by the TG results. However, pyrolysis tests in the semi-continuous reactor showed similar solid yields for all tests, with the values of this parameter varying only between -6 and +9% for the catalytic tests, compared with the non-catalytic mixture, therefore showing a reduced effect of the minerals on the mass loss for higher-scale tests.

Natural minerals also significantly changed the kinetic parameters of the pyrolysis process, drastically decreasing the apparent activation energies of the catalytic mixtures compared with the quartz sand mixture. Calcination of the natural minerals promoted an even more prominent decrease of the $E_a$, with values between 85 and 130 kJ/mol for the mixtures with C-Dolomite and C-Clinoptilolite, which are even lower than the apparent activation energies obtained for pure orange peel at similar conversion degrees. The kinetic constant $k$ also increased with calcination of the catalysts, which shows this thermal treatment proves positive from a kinetic approach.

The calcination treatment showed to shift selectivity of products, with higher content of less-oxygenated compounds found in C-Dolomite and C-Clinoptilolite, compared with the tests where non-calcined minerals were used. On the other hand, hydrogen production was higher for C-Clinoptilolite, while C-Dolomite showed higher selectivity for methane production than its non-calcined counterpart. Therefore, high potential for the use of natural, cheap and abundant materials such as dolomite and zeolite has been found; future studies will focus on the use of different natural minerals, along with simple, chemical modification of the functional groups present in these materials.

## ACKNOWLEDGMENTS

This research is a product of the Project 266632 "Laboratorio Binacional para la Gestión Inteligente de la Sustentabilidad Energética y la Formación Tecnológica" ["Bi-National Laboratory on Smart Sustainable Energy Management and Technology Training"], funded by the CONACYT SENER Fund for Energy Sustainability (Agreement: S0019 201401).

## CONFLICT OF INTEREST

The authors have no conflicts of interest to declare.

## REFERENCES

Adam, J., Antonakou, E., Lappas, A., Stöcker, M., Nilsen, M. H., Bouzga, A., … Øye, G. (2006). In situ catalytic upgrading of biomass derived fast pyrolysis vapours in a fixed bed reactor using mesoporous materials. *Microporous and Mesoporous Materials*, *96*(1), 93–101. https://doi.org/10.1016/j.micromeso.2006.06.021

Adriano Macas, A. F. (2012). *Absorción y Desorción de Vapor de Agua mediante la utilización de las Zeolitas Naturales de la Provincia de Guayas*. Escuela Superior Politécnica del Litoral.

Aguiar, L., Márquez-Montesinos, F., Gonzalo, A., Sánchez, J. L., & Arauzo, J. (2008). Influence of temperature and particle size on the fixed bed pyrolysis of orange peel residues. *Journal of Analytical and Applied Pyrolysis*, *83*(1), 124–130. https://doi.org/10.1016/j.jaap.2008.06.009

Aho, A., Kumar, N., Eränen, K., Salmi, T., Hupa, M., & Murzin, D. Y. (2007). Catalytic Pyrolysis of Biomass in a Fluidized Bed Reactor: Influence of the Acidity of H-Beta Zeolite. *Process Safety and Environmental Protection*, *85*(5), 473–480. https://doi.org/10.1205/psep07012

Aho, A., Kumar, N., Eränen, K., Salmi, T., Hupa, M., & Murzin, D. Y. (2008). Catalytic pyrolysis of woody biomass in a fluidized bed reactor: Influence of the zeolite structure. *Fuel*, *87*(12), 2493–2501. https://doi.org/10.1016/j.fuel.2008.02.015

Algoufi, Y. T., Kabir, G., & Hameed, B. H. (2017). Synthesis of glycerol carbonate from biodiesel by-product glycerol over calcined dolomite. *Journal of the Taiwan Institute of Chemical Engineers*, *70*, 179–187. https://doi.org/10.1016/j.jtice.2016.10.039

Antonakou, E., Lappas, A., Nilsen, M. H., Bouzga, A., & Stöcker, M. (2006). Evaluation of various types of Al-MCM-41 materials as catalysts in biomass pyrolysis for the production of bio-fuels and chemicals. *Fuel*, *85*(14), 2202–2212. https://doi.org/10.1016/j.fuel.2006.03.021

Ates, A., & Hardacre, C. (2012). The effect of various treatment conditions on natural zeolites: Ion exchange, acidic, thermal and steam treatments. *Journal of Colloid and Interface Science*, *372*(1), 130–140. https://doi.org/10.1016/j.jcis.2012.01.017

Atutxa, A., Aguado, R., Gayubo, A. G., Olazar, M., & Bilbao, J. (2005). Kinetic Description of the Catalytic Pyrolysis of Biomass in a Conical Spouted Bed Reactor. *Energy & Fuels*, *19*(3), 765–774. https://doi.org/10.1021/ef040070h

Babich, I. V, van der Hulst, M., Lefferts, L., Moulijn, J. A., O'Connor, P., & Seshan, K. (2011). Catalytic pyrolysis of microalgae to high-quality liquid bio-fuels. *Biomass and Bioenergy*, *35*(7), 3199–3207. https://doi.org/10.1016/j.biombioe.2011.04.043

Bridgwater, T. (2006). Biomass for energy. *Journal of the Science of Food and Agriculture*, *86*(12), 1755–1768. https://doi.org/10.1002/jsfa.2605

Bridgwater, A. V. (1996). Production of high grade fuels and chemicals from catalytic pyrolysis of biomass. *Catalysis Today*, *29*(1), 285–295. https://doi.org/10.1016/0920-5861(95)00294-4

Bridgwater, A. V, & Peacocke, G. V. C. (2000). Fast pyrolysis processes for biomass. *Renewable and Sustainable Energy Reviews*, *4*(1), 1–73. https://www.sciencedirect.com/science/article/pii/S1364032199000076

Charusiri, W., & Vitidsant, T. (2017). Upgrading bio-oil produced from the catalytic pyrolysis of sugarcane (Saccharum officinarum L) straw using calcined dolomite. *Sustainable Chemistry and Pharmacy*, *6*, 114–123. https://doi.org/https://doi.org/10.1016/j.scp.2017.10.005

Conesa, J. A., & Domene, A. (2015). Gasification and pyrolysis of Posidonia oceanica in the presence of dolomite. *Journal of Analytical and Applied Pyrolysis*, *113*, 680–689. https://www.sciencedirect.com/science/article/pii/S0165237015300280

Corma, A., Huber, G. W., Sauvanaud, L., & O'Connor, P. (2007). Processing biomass-derived oxygenates in the oil refinery: Catalytic cracking (FCC) reaction pathways and role of catalyst. *Journal of Catalysis*, *247*(2), 307–327.

Correia, L. M., de Sousa Campelo, N., Novaes, D. S., Cavalcante, C. L., Cecilia, J. A., Rodríguez-Castellón, E., & Vieira, R. S. (2015). Characterization and application of dolomite as catalytic precursor for canola and sunflower oils for biodiesel production. *Chemical Engineering Journal*, *269*, 35–43.

De J. Montes Luna, A., de León, G. C., Rodríguez, S. P. G., López, N. C. F., Camacho, O. P., & Mercado, Y. A. P. (2018). Na+/Ca2+ aqueous ion exchange in natural clinoptilolite zeolite for polymer-zeolite composite membranes production and their CH4/CO2/N2 separation performance. *Journal of Natural Gas Science and Engineering*, *54*, 47–53.

Demiral, I., & Sensöz, S. (2008). The effects of different catalysts on the pyrolysis of industrial wastes (olive and hazelnut bagasse). *Bioresource Technology*, *99*(17), 8002—8007. https://doi.org/10.1016/j.biortech.2008.03.053

Djayaprabha, H. S., Chang, T. P., Shih, J. Y., & Chen, C. T. (2017). Mechanical properties and microstructural analysis of slag based cementitious binder with calcined dolomite as an activator. *Construction and Building Materials*, *150*, 345–354. https://doi.org/10.1016/j.conbuildmat.2017.05.221

E.F. Iliopoulou, E.V. Antonakou, S.A. Karakoulia, I.A. Vasalos, A.A. Lappas, K. S. T. (2007). Catalytic conversion of biomass pyrolysis products by mesoporous materials: Effect of steam stability and acidity of Al-MCM-41 catalysts. *Chemical Engineering Journal*, *134*(1), 51–57.

Elbaba, I. F., & Williams, P. T. (2013). High yield hydrogen from the pyrolysis–catalytic gasification of waste tyres with a nickel/dolomite catalyst. *Fuel*, *106*, 528–536.

Faghihian, H., Talebi, M., & Pirouzi, M. (2008). Adsorption of nitrogen from natural gas by clinoptilolite. *Journal of the Iranian Chemical Society*, *5*(3), 394–399. https://doi.org/10.1007/BF03245993

Favvas, E. P., Tsanaktsidis, C. G., Sapalidis, A. A., Tzilantonis, G. T., Papageorgiou, S. K., & Mitropoulos, A. C. (2016). Clinoptilolite, a natural zeolite material: Structural characterization and performance evaluation on its dehydration properties of hydrocarbon-based fuels. *Microporous and Mesoporous Materials*, *225*, 385–391.

French, R., & Czernik, S. (2010). Catalytic pyrolysis of biomass for biofuels production. *Fuel Processing Technology*, *91*(1), 25–32.

Guillory, J. K. (2010). Book Review of CRC Handbook of Chemistry and Physics. 91st Edition. *Journal of Medicinal Chemistry*, *53*(24), 8780. https://doi.org/10.1021/jm101422n

Guvenir, Ö. (2005). *Synthesis and characterization of clinoptilolite*. The Middle East Technical University.

Helwani, Z., Othman, M. R., Aziz, N., Fernando, W. J. N., & Kim, J. (2009). Technologies for production of biodiesel focusing on green catalytic techniques: A review. *Fuel Processing Technology*, *90*(12), 1502–1514.

Horne, P. A., & Williams, P. T. (1996). Upgrading of biomass-derived pyrolytic vapours over zeolite ZSM-5 catalyst: effect of catalyst dilution on product yields. *Fuel*, *75*(9), 1043–1050.

Huber, G. W., & Corma, A. (n.d.). Synergies between Bio- and Oil Refineries for the Production of Fuels from Biomass. *Angewandte Chemie International Edition*, *46*(38), 7184–7201. https://doi.org/10.1002/anie.200604504

Jain, A. A., Mehra, A., & Ranade, V. V. (2016). Processing of TGA data : Analysis of isoconversional and model fitting methods. *Fuel*, *165*, 490–498. https://doi.org/10.1016/j.fuel.2015.10.042

Jarrahian, K., Seiedi, O., Sheykhan, M., Sefti, M. V., & Ayatollahi, S. (2012). Wettability alteration of carbonate rocks by surfactants: A mechanistic study. *Colloids and Surfaces A: Physicochemical and Engineering Aspects*, *410*, 1–10.

Ji, J., Ge, Y., Balsam, W., Damuth, J. E., & Chen, J. (2009). Rapid identification of dolomite using a Fourier Transform Infrared Spectrophotometer (FTIR): A fast method for identifying Heinrich events in IODP Site U1308. *Marine Geology*, *258*(1), 60–68.

Kantar, S. El, Boussetta, N., Rajha, H. N., Maroun, R. G., Louka, N., & Vorobiev, E. (2018). High voltage electrical discharges combined with enzymatic hydrolysis for extraction of polyphenols and fermentable sugars from orange peels. *Food Research International*.

Kelkar, S., Saffron, C. M., Li, Z., Kim, S.-S., Pinnavaia, T. J., Miller, D. J., & Kriegel, R. (2014). Aromatics from biomass pyrolysis vapour using a bifunctional mesoporous catalyst. *Green Chem.*, *16*(2), 803–812. https://doi.org/10.1039/C3GC41350K

Kersten, S. R. A., van Swaaij, W. P. M., Lefferts, L., & Seshan, K. (2007). Options for Catalysis in the Thermochemical Conversion of Biomass into Fuels. In *Catalysis for Renewables* (pp. 119–145). Wiley-Blackwell. https://doi.org/10.1002/9783527621118.ch6

Kim, J.-C., Lee, S., Cho, K., Na, K., Lee, C., & Ryoo, R. (2014). Mesoporous MFI Zeolite Nanosponge Supporting Cobalt Nanoparticles as a Fischer–Tropsch Catalyst with High Yield of Branched Hydrocarbons in the Gasoline Range. *ACS Catalysis*, *4*(11), 3919–3927. https://doi.org/10.1021/cs500784v

Kim, Y.-M., Lee, H. W., Jae, J., Jung, K. Bin, Jung, S.-C., Watanabe, A., & Park, Y.-K. (2017). Catalytic co-pyrolysis of biomass carbohydrates with LLDPE over Al-SBA-15 and mesoporous ZSM-5. *Catalysis Today*, *298*, 46–52.

Korkuna, O., Leboda, R., Skubiszewska-Zie¸ba, J., Vrublevs'ka, T., Gun'ko, V. M., & Ryczkowski, J. (2006). Structural and physicochemical properties of natural zeolites: clinoptilolite and mordenite. *Microporous and Mesoporous Materials*, *87*(3), 243–254.

Lappas, A. A., Samolada, M. C., Iatridis, D. K., Voutetakis, S. S., & Vasalos, I. A. (2002). Biomass pyrolysis in a circulating fluid bed reactor for the production of fuels and chemicals. *Fuel*, *81*(16), 2087–2095.

Lavat, A. E., Grasselli, M. C., & Lovecchio, E. G. (2015). The firing steps and phases formed in Mg–Zr–Al refractory dolomite-based materials. *Ceramics International*, *41*(2, Part A), 2107–2115.

Lazdovica, K., Liepina, L., & Kampars, V. (2015). Comparative wheat straw catalytic pyrolysis in the presence of zeolites, Pt/C, and Pd/C by using TGA-FTIR method. *Fuel Processing Technology*, *138*, 645–653.

Lazdovica, K., Liepina, L., & Kampars, V. (2016). Catalytic pyrolysis of wheat bran for hydrocarbons production in the presence of zeolites and noble-metals by using TGA-FTIR method. *Bioresource Technology*, *207*, 126–133.

Li, B. B., Smith, B., & Hossain, M. M. (2006). Extraction of phenolics from citrus peels: II. Enzyme-assisted extraction method. *Separation and Purification Technology*, *48*(2), 189–196.

Li, J., Li, X., Zhou, G., Wang, W., Wang, C., Komarneni, S., & Wang, Y. (2014). Catalytic fast pyrolysis of biomass with mesoporous ZSM-5 zeolites prepared by desilication with NaOH solutions. *Applied Catalysis A: General*, *470*, 115–122.

Listing Compounds. (n.d.). Retrieved from http://foodb.ca/compounds

Lopez-Velazquez, M. A., Santes, V., Balmaseda, J., & Torres-Garcia, E. (2013a). Pyrolysis of orange waste: A thermo-kinetic study. *Journal of Analytical and Applied Pyrolysis*, *99*, 170–177.

Lopez-Velazquez, M. A., Santes, V., Balmaseda, J., & Torres-Garcia, E. (2013b). Pyrolysis of orange waste: A thermo-kinetic study.

*Journal of Analytical and Applied Pyrolysis*, *99*, 170–177. https://doi.org/10.1016/j.jaap.2012.09.016

Luengo, E., Álvarez, I., & Raso, J. (2013). Improving the pressing extraction of polyphenols of orange peel by pulsed electric fields. *Innovative Food Science & Emerging Technologies*, *17*, 79–84.

Maran, J. P., Sivakumar, V., Thirugnanasambandham, K., & Sridhar, R. (2013). Optimization of microwave assisted extraction of pectin from orange peel. *Carbohydrate Polymers*, *97*(2), 703–709.

Marshall, R. E., & Farahbakhsh, K. (2013). Systems approaches to integrated solid waste management in developing countries. *Waste Management*, *33*(4), 988–1003.

Messina, L. I. G., Bonelli, P. R., & Cukierman, A. L. (2017). In-situ catalytic pyrolysis of peanut shells using modified natural zeolite. *Fuel Processing Technology*, *159*, 160–167.

Miranda, R., Bustos-Martinez, D., Blanco, C. S., Villarreal, M. H. G., & Cantú, M. E. R. (2009a). Pyrolysis of sweet orange (Citrus sinensis) dry peel. *Journal of Analytical and Applied Pyrolysis*, *86*(2), 245–251. https://doi.org/10.1016/j.jaap.2009.06.001

Miranda, R., Bustos-Martinez, D., Blanco, C. S., Villarreal, M. H. G., & Cantú, M. E. R. (2009b). Pyrolysis of sweet orange (Citrus sinensis) dry peel. *Journal of Analytical and Applied Pyrolysis*, *86*(2), 245–251.

Nguyen, T. S., Zabeti, M., Lefferts, L., Brem, G., & Seshan, K. (2013). Catalytic upgrading of biomass pyrolysis vapours using faujasite zeolite catalysts. *Biomass and Bioenergy*, *48*, 100–110.

Nokkosmäki, M. I., Krause, A. O. I., Leppämäki, E. A., & Kuoppala, E. T. (1998). A novel test method for catalysts in the treatment of biomass pyrolysis oil. *Catalysis Today*, *45*(1), 405–409.

Olguín Gutiérrez, M. T. (2007). *Zeolitas. Características y propiedades*. México, D.F.

Paulo, C., & Dittrich, M. (2013). 2D Raman spectroscopy study of dolomite and cyanobacterial extracellular polymeric substances from Khor Al-Adaid sabkha (Qatar). *Journal of Raman Spectroscopy*, *44*(11), 1563–1569. https://doi.org/10.1002/jrs.4368

Pearce, P. J., & Simkins, R. J. J. (1968). Acid strengths of some substituted picric acids. *Canadian Journal of Chemistry*, *46*(2), 241–248. https://doi.org/10.1139/v68-038

Pereira, C. G., Féjean, C., Betoulle, S., Ferrando, N., Lugo, R., de Hemptinne, J. C., & Mougin, P. (2018). Guaiacol and its mixtures: New data and predictive models part 1: Phase equilibrium. *Fluid Phase Equilibria*.

Perraki, T., & Orfanoudaki, A. (2004). Mineralogical study of zeolites from Pentalofos area, Thrace, Greece. *Applied Clay Science*, *25*(1), 9–16.

Pütün, E., Uzun, B. B., & Pütün, A. E. (2006). Fixed-bed catalytic pyrolysis of cotton-seed cake: effects of pyrolysis temperature, natural zeolite content and sweeping gas flow rate. *Bioresource Technology*, *97*(5), 701—710. https://doi.org/10.1016/j.biortech.2005.04.005

Ranzi, E., Cuoci, A., Faravelli, T., Frassoldati, A., Migliavacca, G., Pierucci, S., & Sommariva, S. (2008). Chemical Kinetics of Biomass Pyrolysis. *Energy & Fuels*, *22*(6), 4292–4300. https://doi.org/10.1021/ef800551t

Rodríguez-Méndez, B. G., López-Callejas, R., Olguín, M. T., Hernández-Arias, A. N., Valencia-Alvarado, R., Pena-Eguiluz, R., … De La Piedad-Beneitez, A. (2014). Bacterial inactivation in water by means of a combined process of pulsed dielectric barrier discharge and silver-modified natural zeolite. *Journal of Physics D: Applied Physics*, *47*(23). https://doi.org/10.1088/0022-3727/47/23/235401

SAGARPA, Secretary of Agriculture, Livestock, Rural development, F. and F. (n.d.). No Title. Retrieved April 13, 2018.

Santos, C. M., Dweck, J., Viotto, R. S., Rosa, A. H., & de Morais, L. C. (2015). Application of orange peel waste in the production of solid biofuels and biosorbents. *Bioresource Technology*, *196*, 469–479. https://doi.org/10.1016/j.biortech.2015.07.114

Sasaki, K., Yoshida, M., Ahmmad, B., Fukumoto, N., & Hirajima, T. (2013). Sorption of fluoride on partially calcined dolomite. *Colloids and Surfaces A: Physicochemical and Engineering Aspects*, *435*, 56–62.

Scognamiglio, J., Jones, L., Letizia, C. S., & Api, A. M. (2012). Fragrance material review on cyclotene propionate. *Food and Chemical Toxicology*, *50*, S592–S595.

Serjeant, E. P., & Dempsey, B. (1979). *Ionisation constants of organic acids in aqueous solution* (Internatio). New York: Oxford ; New York : Pergamon Press.

Shiu, W.-Y., Ma, K.-C., Varhaníčková, D., & Mackay, D. (1994). Chlorophenols and alkylphenols: A review and correlation of environmentally relevant properties and fate in an evaluative environment. *Chemosphere*, *29*(6), 1155–1224.

Starink, M. J. (2003). The determination of activation energy from linear heating rate experiments : a comparison of the accuracy of isoconversion methods, *404*, 163–176. https://doi.org/10.1016/S0040-6031(03)00144-8

Suárez-Jacobo, A., Alcantar-Rosales, V. M., Alonso-Segura, D., Heras-Ramírez, M., Rosa, D. E.-D. La, Lugo-Melchor, O., & Gaspar-Ramirez, O. (2017). Pesticide residues in orange fruit from citrus orchards in Nuevo Leon State, Mexico. *Food Additives & Contaminants: Part B*, *10*(3), 192–199. https://doi.org/10.1080/19393210.2017.1315743

Urych, B. (2014). Determination of Kinetic Parameters of Coal Pyrolysis to Simulate the Process of Underground Coal Gasification (UCG). *Journal of Sustainable Mining*, *13*(1), 3–9. https://doi.org/10.7424/jsm140102

Venkatesh, M., Ravi, P., & Tewari, S. P. (2013). Isoconversional Kinetic Analysis of Decomposition of Nitroimidazoles: Friedman method vs Flynn–Wall–Ozawa Method. *The Journal of Physical Chemistry A*, *117*(40), 10162–10169. https://doi.org/10.1021/jp407526r

Veses, A., Aznar, M., Martínez, I., Martínez, J. D., López, J. M., Navarro, M. V, … García, T. (2014). Catalytic pyrolysis of wood biomass in an auger reactor using calcium-based catalysts. *Bioresource Technology*, *162*, 250–258.

Vieira, A. J., Beserra, F. P., Souza, M. C., Totti, B. M., & Rozza, A. L. (2018). Limonene: Aroma of innovation in health and disease. *Chemico-Biological Interactions*, *283*, 97–106.

Vitolo, S., Seggiani, M., Frediani, P., Ambrosini, G., & Politi, L. (1999). Catalytic upgrading of pyrolytic oils to fuel over different zeolites. *Fuel*, *78*(10), 1147–1159.

Wang, D., Xiao, R., Zhang, H., & He, G. (2010). Comparison of catalytic pyrolysis of biomass with MCM-41 and CaO catalysts by using TGA–FTIR analysis. *Journal of Analytical and Applied Pyrolysis*, *89*(2), 171–177.

Wang, Y., Yokoi, T., Namba, S., & Tatsumi, T. (2016). Effects of Dealumination and Desilication of Beta Zeolite on Catalytic Performance in n -Hexane Cracking, 1–19.

Widyawati, M., Church, T. L., Florin, N. H., & Harris, A. T. (2011). Hydrogen synthesis from biomass pyrolysis with in situ carbon dioxide capture using calcium oxide. *International Journal of Hydrogen Energy*, *36*(8), 4800–4813.

Xie, J., Chen, T., Xing, B., Liu, H., Xie, Q., Li, H., & Wu, Y. (2016). The thermochemical activity of dolomite occurred in dolomite–palygorskite. *Applied Clay Science*, *119*, 42–48.

Yaman, S. (2004). Pyrolysis of biomass to produce fuels and chemical feedstocks. *Energy Conversion and Management*, *45*(5), 651–671.

Yeast Metabolome Database. (n.d.).

Zhang, Y., Xiao, R., Gu, X., Zhang, H., Shen, D., & He, G. (2014). Catalytic pyrolysis of biomass with Fe/La/SBA-15 catalyst using TGA–FTIR analysis. *BioResources*, *9*(3), 5234-5245.

Zhao, H. Y., Li, D., Bui, P., & Oyama, S. T. (2011). Hydrodeoxygenation of guaiacol as model compound for pyrolysis oil on transition metal phosphide hydroprocessing catalysts. *Applied Catalysis A: General*, *391*(1), 305–310.